

Discovery of the benchmark metal poor T8 dwarf BD+01 2920B

D. J. Pinfield^{1*}, B. Burningham¹, N. Lodieu^{2,3}, S. K. Leggett⁴, C. G. Tinney⁵, L. van Spaandonk¹, F. Marocco¹, R. Smart⁶, J. Gomes¹, L. Smith¹, P. W. Lucas¹, A. C. Day-Jones⁷, D. N. Murray¹, A. C. Katsiyannis⁸, S. Catalan¹, C. Cardoso^{6,1,9}, J. R. A. Clarke¹, S. Folkes¹⁰, M. C. Gálvez-Ortiz¹¹, D. Homeier¹², J. S. Jenkins⁷, H. R. A. Jones¹, Z. H. Zhang¹

¹Centre for Astrophysics Research, Science and Technology Research Institute, University of Hertfordshire, Hatfield AL10 9AB

²Instituto de Astrofísica de Canarias, Vía Láctea s/n, E-38205 La Laguna, Tenerife, Spain

³Departamento de Astrofísica, Universidad de La Laguna (ULL), E-38205 La Laguna, Tenerife, Spain

⁴Gemini Observatory, 670 N. A‘ohoku Place, Hilo, HI 96720, USA

⁵Department of Astrophysics, School of Physics, University of New South Wales, NSW 2052, Australia

⁶Istituto Nazionale di Astrofisica, Osservatorio Astronomico di Torino, Strada Osservatorio 20, 10025 Pino Torinese, Italy

⁷Universidad de Chile, Santiago, Casilla 36-D, Chile

⁸Institute of Astronomy & Astrophysics, National Observatory of Athens, Penteli, GR-15236, Greece

⁹Astrophysics Group, College of Engineering, Mathematics, and Physical Sciences, University of Exeter, Exeter EX4 4QL, UK

¹⁰Departamento de Física y Astronomía, Universidad de Valparaíso, Av. Gran Bretaña 1111, Casilla 5030, Valparaíso, Chile

¹¹Centro de Astrobiología (CSIC-INTA), Ctra. Ajalvir km 4, E-28850 Torrejón de Ardoz, Madrid, Spain

¹²CRAL, UMR 5574, CNRS, Université de Lyon, École Normale Supérieure de Lyon, 46 Allée d’Italie, 69364 Lyon Cédex 07, France

15 November 2018

ABSTRACT

We have searched the WISE first data release for widely separated ($\leq 10,000$ AU) late T dwarf companions to Hipparcos and Gliese stars. We have discovered a new binary system containing a K-band suppressed T8p dwarf WISEP J1423+0116 and the mildly metal poor ($[\text{Fe}/\text{H}] = -0.38 \pm 0.06$) primary BD+01 2920 (Hip 70319), a G1 dwarf at a distance of 17.2 pc. This new benchmark has $T_{\text{eff}} = 680 \pm 55$ K and a mass of $20 - 50 M_{\text{Jup}}$. Its spectral properties are well modelled except for known discrepancies in the Y and K bands. Based on the well determined metallicity of its companion, the properties of BD+01 2920B imply that the currently known T dwarfs are dominated by young low-mass objects. We also present an accurate proper motion for the T8.5 dwarf WISEP J075003.84+272544.8.

Key words: surveys - stars: low-mass, brown dwarfs

1 INTRODUCTION

An accurate understanding of the physics of ultra-cool atmospheres ($T_{\text{eff}} < 2300$ K) is a major and ongoing challenge for theory (e.g. Allard et al. 1997). Complex molecular opacities (e.g. Barber et al. 2006), condensate clouds and their properties (e.g. Allard et al. 2001), and non-equilibrium chemistry (i.e. vertical transport or mixing; Saumon et al. 2007) are significant sources of uncertainty in the models. However, it is crucial to improve our understanding if we are to effectively measure the properties of substellar populations (brown dwarfs and giant planets) and study their formation

and evolution (e.g. Bate et al. 2002; Goodwin & Whitworth 2007; Stamatellos et al. 2007; Sumi et al. 2011).

Building on the samples of L (~ 2300 K– 1500 K) and T dwarfs (~ 1500 K– 500 K) (Kirkpatrick 2005) identified in the Two-Micron All Sky Survey (Skrutskie et al. 2006), the DENIS survey (Epchtein et al. 1997) and the Sloan Digital Sky Survey (York et al. 2000), a new generation of infrared surveys is expanding our search-space into much greater volumes. The UKIRT Infrared Deep Sky Survey (UKIDSS; Lawrence et al. 2007) is sensitive to mid L – mid T dwarfs out to ~ 100 pc over $\sim 15\%$ of the sky. The VISTA surveys (e.g. the Viking and VHS surveys) will expand this coverage to $\sim 50\%$ of the sky in the next few years. For the latest T dwarfs (T8-9; e.g. Warren et al. 2007; Burningham et al. 2008; Delorme et al. 2008; Lucas et al.

* E-mail: D.J.Pinfield@herts.ac.uk

2010; Burningham et al. 2011c) the sensitivities of these surveys are matched by those of the Wide-field Infrared Survey Explorer (WISE; Wright et al. 2010), probing to distances of $\sim 15\text{--}25\text{pc}$. And for even lower temperatures ($T_{\text{eff}} < 500\text{K}$) an increased mid-/near-infrared flux ratio is allowing WISE to uncover the new Y dwarf class in the $\sim 300\text{--}500\text{K}$ range (Cushing et al. 2011). Together these surveys are characterising a rapidly growing population in the near- and mid-infrared (e.g. Lodieu et al. 2007; Pinfield et al. 2008; Burningham et al. 2010b; Reyl   et al. 2010; Kirkpatrick et al. 2011).

With sensitivity to a growing field L-, T- and Y-dwarf search-space it is becoming feasible to search for multiple systems (e.g. Burningham et al. 2009a; Zhang et al. 2010; Burningham et al. 2010a; Day-Jones et al. 2011; Murray et al. 2011; Burningham et al. 2011a; Leggett et al. 2010c) or moving group associations (e.g. Clarke et al. 2010; G  lvez-Ortiz et al. 2010). The physical properties (mass, age and metallicity) of such objects can be constrained through association with more readily characterisable stellar companions or moving group members, establishing them as benchmark objects that can test the theory or more directly map physical properties onto spectral characteristics (e.g. Pinfield et al. 2006). Indeed, by searching for even rarer benchmarks with better physical constraints which span a more extreme range of properties, it will be possible to provide the strongest tests for the model atmospheres, a goal that absolutely requires sensitivity to large volumes.

In this paper we present a search of the WISE first data release for widely separated late T dwarf companions to stars with known parallaxes. Section 2 describes our WISE sample selection, and Section 3 the method used to identify candidate binary associations. Sections 4 and 5 present our spectroscopic and additional photometric data, and in Section 6 we derive candidate proper motions. Section 7 statistically assesses the expected level of false positives in our search, and Sections 8, 9 and 10 discuss the properties and characteristics of a newly discovered benchmark system. Conclusions and future work are in Section 11.

2 WISE SAMPLE

We identified candidate mid-T and later type objects in the WISE Preliminary Data Release source catalogue, which we accessed via the NASA/IPAC Infrared Science Archive’s catalogue query engine. We performed a series of all-sky searches using structured query language input to select sources with constraints on signal-to-noise and colour, and with detections in various combinations of bands chosen to optimise sensitivity to late T dwarfs. We always required a detection in the W2-band with signal-to-noise (SNR) of at least 10. If W1- and W2-band detections are available then we require $W1 - W2 \geq 2.0$ to select spectral types of $>T5$ (Kirkpatrick et al. 2011; Mainzer et al. 2011). If W2- and W3-band detections are available then we require $W2 - W3 \leq 2.5$ in order to avoid dusty galaxies such as ULIRGS, LINERS and obscured AGN (Wright et al. 2010). As well as our WISE-band detection requirements we also made use of the WISE catalogue cross-match with the 2MASS point source catalogue, to divide our searches into objects that are detected in 2MASS (within 3 arcseconds

of the WISE position) and those that are not. For 2MASS detected objects we required that either $H - W2 \geq 2.5$ or $J - W2 \geq 3.5$ so as to remove L and early T dwarfs. The full complement of searches and the number of sources identified in each is shown in Table 1.

The search requiring detection in only the W2-band will be the most sensitive to faint objects with red WISE colours since the WISE sensitivity limits (all-sky $5\text{-}\sigma$ Vega limits are $W1=16.5$, $W2=15.5$, $W3=11.2$, $W4=7.9$; Wright et al. 2010) mean that objects with $W1 - W2 > 2$ will generally only be detected in W2 for $W2=14.5\text{--}15.5$ (i.e. at least $\sim 75\%$ of the W2 survey volume). The other multi-band combinations cover the full range of detection/non-detection combinations that might be expected for T dwarfs.

For comparison, the recent large-scale WISE search made by Kirkpatrick et al. (2011) overlaps significantly with our search-space. However, they use a slightly bluer $W1 - W2 \geq 1.5$ selection, and where we require $\text{SNR} > 10$ in the W2-band they require at least 8 separate detections ($\text{SNR} > 3$) in the individual W2 exposures.

3 IDENTIFYING CANDIDATE BINARY SYSTEMS

To identify candidate binary systems we cross-matched our candidate late-T sample with a list of potential primary stars with measured parallax distances, and imposed separation constraints on the potential binary pairings as well as absolute magnitude constraints on the candidate T dwarfs (where we assumed a common distance for components). The list of potential primary stars was made by combining together the latest Hipparcos catalogue (van Leeuwen 2007) with the most recent version of the catalogue of nearby stars (Gliese & Jahreiss 1991). Hipparcos provides astrometric measurements (in position, parallax, and annual proper motion) with uncertainties in the range 0.7-0.9 milliarcsec (mas) for stars brighter than $V=9$. The catalogue is on the ICRS reference system and has proper motions consistent with an inertial system at the level of $\pm 0.25\text{mas/yr}$. The Third Catalogue of Nearby Stars (CNS3) contains information on all known stars within 25 parsecs based on an extensive literature search during almost four decades.

We required on-sky angular separation of candidate pairs to be ≤ 300 arcseconds to reduce contamination from random alignments, and physical separation of $\leq 10,000\text{AU}$ (where we use the distance of the primary to convert angular separation into a physical line-of-sight separation), since the great majority of known wide ultracool stellar companions have separations below this limit (e.g. Zhang et al. 2010; Faherty et al. 2010). In addition we use the known distance of each candidate primary to estimate the M_{W2} that the T dwarf candidate would have at this distance, and reject any associations where the T dwarf candidate would have $M_{W2} \leq 11.5$ (i.e. targeting late T dwarf companions, e.g. Fig 4 of Leggett et al. 2010a, where $M_{[4.5]}$ is a good proxy for M_{W2}). The candidate T dwarf components of the possible binary systems are distributed within our WISE source selections as summarised in Table 1. These T dwarf candidates were visually inspected using the WISE image server at the NASA/IPAC Infrared Science Archive, and candidates rejected if the source did not appear point-like in any of the

WISE detection?			Colours		Selected sources ^d	Candidate companions ^{d,e}	Selected sources ^f	Candidate companions ^f
W1	W2 ^a	W3	W4					
n ^b	Y ^c	n	n	-	2418	12(3)	289	0
Y	Y	n	n	$W1 - W2 \geq 2.0$	5622	35(1)	1330	0
Y	Y	Y	n	$W1 - W2 \geq 2.0$ $W2 - W3 \leq 2.5$	1721	9(1)	283	0
Y	Y	Y	Y	$W1 - W2 \geq 2.0$ $W2 - W3 \leq 2.5$	1018	2	1642	0
n	Y	Y	n	$W2 - W3 \leq 2.5$	174	0	54	0
n	Y	Y	Y	$W2 - W3 \leq 2.5$	272	0	54	0

^a W2 signal-to-noise always >10 ($w2snr >= 10$).

^b Non-detections defined as ($w\star mpro$ is null or $w\star sigmpro$ is null).

^c Detections defined as ($w\star mpro$ is not null and $w\star sigmpro$ is not null).

^d 2MASS non detections ($tmass_key$ is null).

^e The numbers in brackets are for candidates that passed visual inspection.

^f 2MASS detections with $H - W2 \geq 2.5$ or $J - W2 \geq 3.5$.

Table 1. WISE late T candidate sample. Twelve separate selections were made, six requiring non-detection in 2MASS and six requiring 2MASS detection with red 2MASS-WISE colour. The number of candidate T dwarfs, and those that became wide companion candidates (see Section 3) are indicated for each search, where various combinations of detection and non-detection were explored in the four WISE bands.

bands, formed part of a blended structure, or was clearly an artefact (e.g. part of a diffraction spike).

Five candidate binary systems passed visual inspection. One W2-only detected candidate remains an unconfirmed interesting candidate without any additional survey data (e.g. UKIDSS, VISTA) to facilitate proper motion measurements. The other 4 are listed below:

- WISEP J075003.84+272544.8 is a W2-only detected candidate 265 arcseconds from the star Hip 38228, a G5IV star at 22pc. This candidate is a known T8.5 dwarf discovered (with WISE) by Kirkpatrick et al. (2011), though we subsequently show (Section 6) that it is not a companion to Hip 38228.

- WISEP J142320.86+011638.1 (WISEP J1423+0116) is a W2-only detected candidate 153 arcseconds from the star Hip 70319 (BD+01 2920), a G1V star at 17.2pc. It was not identified by Kirkpatrick et al. (2011) because it is only detected in 7 separate W2 exposures in the WISE Preliminary Data Release. This T dwarf is the main subject of this paper.

- WISEP J145715.85-212207.6 is a W1 + W2 + W3 detected candidate near the system Gl 570ABC (Hip 73182 and Hip 73184), a K4V+M1.5V+M3V triple system. This candidate is a known (discovered in 2MASS) T8 member of the multiple system (Burgasser et al. 2000). The WISE catalogue does not list the source as a 2MASS detection because its high proper motion leads to the WISE and 2MASS positions being separated by more than 3 arcseconds.

- WISEP J150457.58+053800.1 is a W1 + W2 detected candidate 63 arcseconds from Hip 73786 (GJ 576), a K8V star at 18.6pc. This candidate is a known (discovered in UKIDSS) T6p companion to this somewhat metal poor star (Murray et al. 2011; Scholz 2010).

Figure 1 shows J - (VISTA) and $W2$ -band images for WISEP J1423+0116, and indicates its separation from the nearby high proper motion star Hip 70319 (BD+01 2920).

4 SPECTROSCOPY

Near-infrared spectroscopy of WISEP J1423+0116 (BD+012920B; see Section 7) was obtained using the Gemini Near InfraRed Spectrograph (GNIRS; Elias et al. 2006) mounted on the Gemini-North telescope on the night of 16th May 2011. The target was observed in cross-dispersed mode capturing the full 0.8–2.5 μ m region with a 1.0'' slit delivering a resolving power of $R \sim 500$. The data were reduced using GNIRS routines in the Gemini IRAF package (Cooke & Rodgers 2005), using the nearby F5V star Hip 63976 for telluric correction. The telluric standard spectrum was divided by a black-body spectrum of an appropriate T_{eff} after removing hydrogen lines by interpolating the local continuum. The rectified standard spectrum was then used to correct for telluric absorption and to provide relative flux calibration. The overlap regions between the orders in the Y -, J - and H -bands agreed well suggesting that the relative flux of the orders is well calibrated. The resulting $YJHK$ spectra are shown in Figure 2.

In Figure 2 we compare our GNIRS spectrum of the new T8 with that of the T8 spectral template 2MASS J04151954-0935066 from Burgasser et al. (2006b). The close similarity of the spectra over most of the wavelength range argues strongly for T8 classification, which is reflected in the values found for the spectral typing flux ratios (see Table 2). Although the new T8 closely traces the T8 template over the 0.9–1.9 μ m range, it displays a considerably more depressed K -band flux, which is interpreted as due to strong collisionally induced absorption by H_2 (CIA H_2 ; Saumon et al. 1994). Increased CIA H_2 is typically attributed to higher pressure atmospheres arising from lower-metallicity and/or high-gravity (e.g. Burgasser et al. 2002; Knapp et al. 2004; Liu et al. 2007). For this reason we assign the type T8p to WISEP J1423+0116, where the 'p' suffix denotes it is pecu-

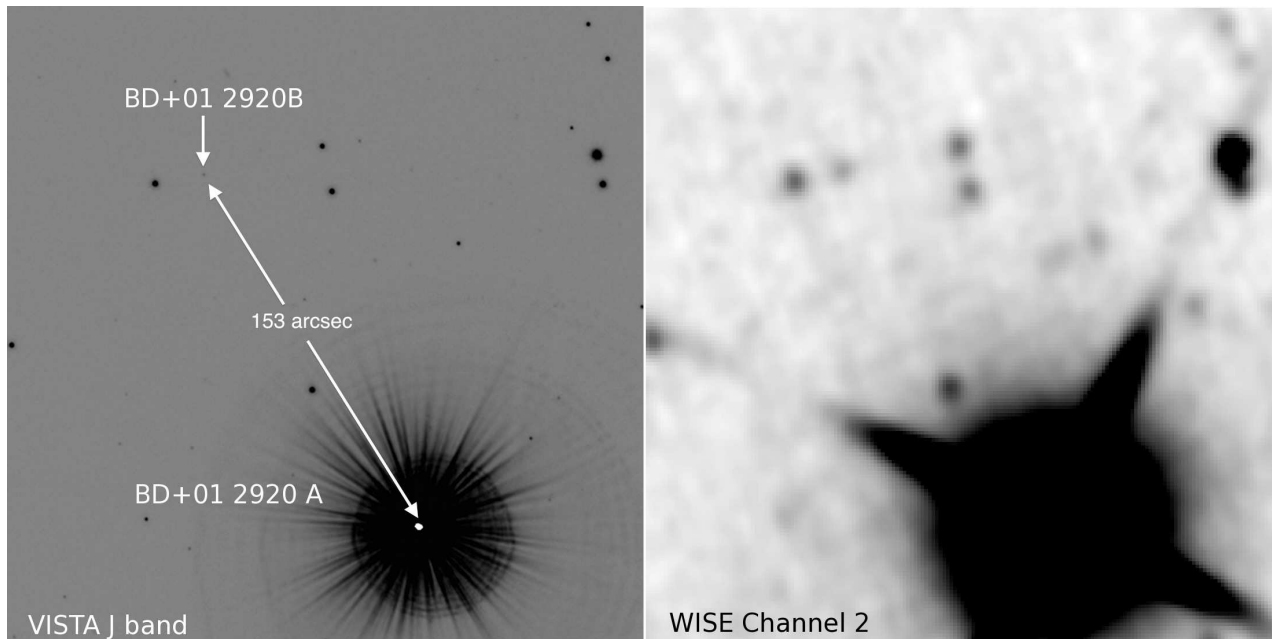


Figure 1. *J*-band and *W2*-band images of WISEP J1423+0116.

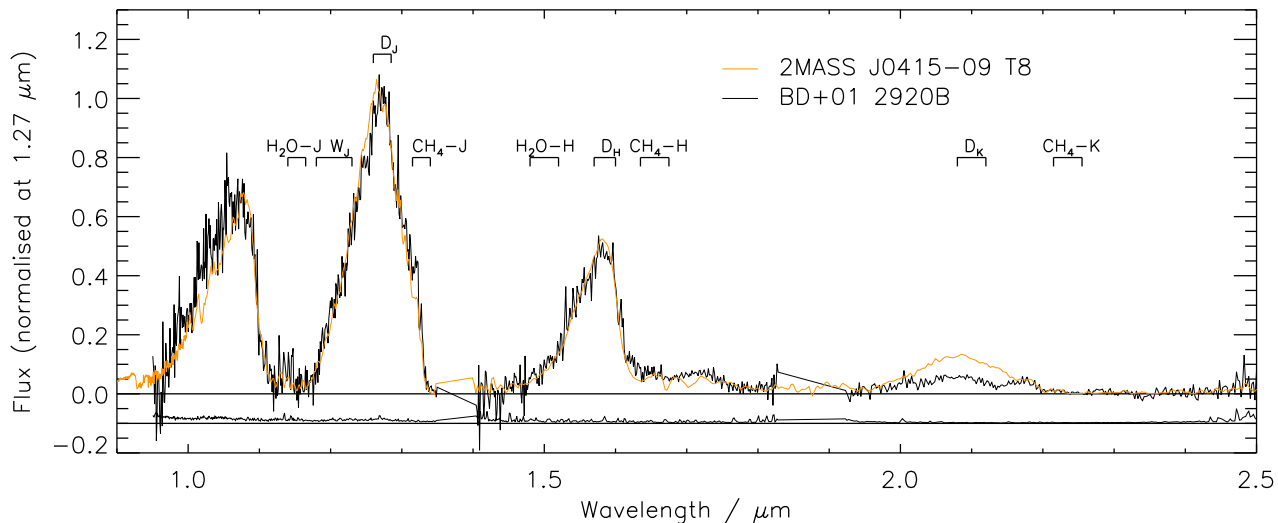


Figure 2. GNIRS spectra for WISEP J1423+0116 (BD+012920B; see Section 7) compared to T8 spectral type template 2MASS J04151954-0935066 taken from Burgasser et al. (2006b). The error spectrum is shown offset by -0.1 .

liar, alluding to the poor match with the template in the *K* band.

5 NEW PHOTOMETRY

Database photometry of WISEP J1423+0116 was obtained from the WISE Preliminary Data Release catalogue, the WFCAM Science Archive (UKIDSS Large Area Survey) and the VISTA Science Archive (VIKING proprietary data access). In addition, observations were taken at the Telescopio Nazionale Galileo (TNG) and with the Spitzer Space Telescope in its warm phase.

Near-infrared photometry was measured using the Near Infrared Camera Spectrometer (NICS; Baffa et al. 2001) at the 3.58-m optical/infrared TNG located on La Palma, on the night of the 7th of May 2011 for the *H* band and the night of the 10th of June 2011 for the *Y* band. The data were obtained in large field mode, with a pixel scale of 0.25 arcsec/pixels and a field of view of 4.2×4.2 arcmins. The data were processed using the NICS science pipeline SNAP provided by the TNG. *H*-band observations consisted of a 50 point jitter pattern with individual 10s exposures and 6 co-adds per jitter point, accumulating to a total exposure time of 50 minutes. In the *Y*-band a 10 point jitter was used

Index	Ratio	Value	Type
H ₂ O-J	$\frac{\int_{1.14}^{1.165} f(\lambda)d\lambda}{\int_{1.26}^{1.285} f(\lambda)d\lambda}$	0.050 ± 0.003	\geq T8
CH ₄ -J	$\frac{\int_{1.315}^{1.34} f(\lambda)d\lambda}{\int_{1.26}^{1.285} f(\lambda)d\lambda}$	0.23 ± 0.01	\geq T8
W_J	$\frac{\int_{1.18}^{1.23} f(\lambda)d\lambda}{2 \int_{1.26}^{1.285} f(\lambda)d\lambda}$	0.32 ± 0.01	T8
H ₂ O-H	$\frac{\int_{1.48}^{1.52} f(\lambda)d\lambda}{\int_{1.56}^{1.60} f(\lambda)d\lambda}$	0.21 ± 0.01	T7/8
CH ₄ -H	$\frac{\int_{1.635}^{1.675} f(\lambda)d\lambda}{\int_{1.56}^{1.60} f(\lambda)d\lambda}$	0.15 ± 0.01	T7/8
NH ₃ -H	$\frac{\int_{1.53}^{1.56} f(\lambda)d\lambda}{\int_{1.57}^{1.60} f(\lambda)d\lambda}$	0.68 ± 0.01	...
CH ₄ -K	$\frac{\int_{2.215}^{2.255} f(\lambda)d\lambda}{\int_{2.08}^{2.12} f(\lambda)d\lambda}$	0.13 ± 0.01	T6/7

Table 2. The spectral flux ratios for WISEP J1423+0116 (BD+012920B; see Section 7). The locations of the numerators and denominators are indicated on Figure 2.

for the same exposure time and co-adds, resulting in a total exposure time of 10 minutes. We calibrated each image onto the MKO system using \sim 30 field stars in the frame.

Warm-Spitzer photometric data were obtained for WISEP J1423+0116 on the 21st August 2011, via the Cycle 7 GO program 70058. Individual frame times were 30 s repeated six times, with a 16-position spiral dither pattern, for a total integration time of 48 min in each of the [3.6] and [4.5] bands. The post-basic-calibrated-data mosaics generated by version 18.18.0 of the Spitzer pipeline were used to obtain aperture photometry. The photometry was derived using a 7-arcsec aperture and the aperture correction was taken from the IRAC handbook. The error is estimated by the larger of either the variation with the sky aperture or the error implied by the uncertainty images.

Tables 3 and 4 contain the available photometry and colours, respectively, for the T dwarf. We present WISE photometry where the signal-to-noise is positive and note that the $W1$ and $W3$ magnitudes are brightness upper limits. The near infrared photometry is on the Mauna-Kea Observatory system (Leggett et al. 2006) except for the TNG Y -filter, which is slightly different ($\lambda_c=1.02\mu\text{m}$, FWHM=0.13 μm) to the MKO Y filter ($\lambda_c=1.02\mu\text{m}$, FWHM=0.10 μm). In the absence of a measured K -band magnitude we have determined a synthetic $J - K$ colour using our GNIRS spectra and a spectrum of Vega (Bohlin & Gilliland 2004) both convolved with the response functions for the pass-bands (e.g. Hewett et al. 2006). This synthetic colour (see Table 4) combined with the J -band magnitude produced our K band estimate. For the mid infrared photometry we note that while similar to $W1$ and $W2$, the Spitzer [3.6] and [4.5] bands have some significant differences (see Fig 2 of Mainzer et al.

2011). There are multiple measurements of Y -, J - and H -band photometry, though no evidence of variability is seen (to within the uncertainties) in the photometric brightness.

6 PROPER MOTIONS

We measured the proper motion of WISEP J1423+0116 using a VISTA VIKING image of April 2010 and two UKIDSS images from May 2008 (with lower signal-to-noise of \sim 6). This avoids using the larger point-spread-functions inherent in the WISE images (\sim 6.5 arcsecs in $W2$). The baseline between the two near infrared epochs was 1.89 years. We took the measured x,y coordinates from the standard CASU pipeline reductions of all images and using 59 objects within 4 arcminutes of the target, transformed the UKIDSS frames onto the standard coordinate system of the VIKING frame using a simple linear model. The relative proper motion for all objects were found from linear fits to the standard coordinates at the different epochs. A correction to an absolute system was estimated from the median difference between measured relative proper motions and 6 SDSS objects in the field with proper motions in the catalog of Munn et al. (2004). The derived proper motion for WISEP J1423+0116 was corrected for an assumed parallax of 50mas (see Section 7), and final uncertainties are based on the formal uncertainties of the measured coordinates combined with an additional allowance for the centroiding accuracy in the low signal-to-noise LAS image ($\sim \pm 0.5$ pixels estimated using Monte Carlo techniques) leading to a proper motion uncertainty of ± 50 mas/yr. The proper motion of WISEP J1423+0116 is $\mu_{\alpha \cos \delta} = 261 \pm 56$ mas yr⁻¹, $\mu_{\delta} = -444 \pm 52$ mas yr⁻¹, which is within 0.7σ of the Hipparcos proper motion vector of Hip 70319 (BD+01 2920; $\mu_{\alpha \cos \delta} = 223.8 \pm 0.4$ mas yr⁻¹, $\mu_{\delta} = -477.4 \pm 0.4$ mas yr⁻¹). These objects are thus a common proper motion pair.

We also measured the proper motion of WISEP J075003.84+272544.8 using two UKIDSS LAS J -band epochs with a baseline of 2 years. We applied a second order polynomial transformation between the two epoch images to correct for any non-uniformity in the focal plane. Seventeen reference stars ($J < 18.1$) were used, distributed around the target (with at least 3 per quadrant) with separations within 2 arcminutes. A correction was applied to an absolute system using apparent proper motions of nearby galaxies. The uncertainties were calculated using the standard deviations in the RA/Dec residuals of sources deemed to have insignificant motion (< 45 milli-arcseconds) between epochs. The proper motion of WISEP J075003.84+272544.8 is $\mu_{\alpha \cos \delta} = -732 \pm 17$ mas yr⁻¹, $\mu_{\delta} = -194 \pm 17$ mas yr⁻¹. By comparison, Kirkpatrick et al. (2011) used astrometric fits to multiple WISE observations to derive a proper motion ($\mu_{\alpha \cos \delta} = -869 \pm 424$ mas yr⁻¹, $\mu_{\delta} = -1107 \pm 438$ mas yr⁻¹) with much larger uncertainties. Their value of $\mu_{\alpha \cos \delta}$ is consistent with our new measurement, however their value of μ_{δ} is too large at the level of $\sim 2\sigma$. Although there also happens to be a nearby Hipparcos star (Hip 38228), it has a low proper motion ($\mu_{\alpha \cos \delta} = -8$ mas yr⁻¹, $\mu_{\delta} = -10$ mas yr⁻¹) and the T dwarf is not a common proper motion companion since its motion differs at a level $> 28\sigma$.

Source	Y^a	J	H	K	$W1(\text{snr})$ or [3.6]	$W2(\text{snr})$ or [4.5]	$W3(\text{snr})$	$W4$
WISE					17.75(1.5) ^b	14.76±0.09(11.8)	12.21(0.8) ^b	-
UKIDSS LAS	19.51±0.14	18.76±0.12						
VISTA VIKING	19.69±0.05	18.71±0.05						
TNG	19.75±0.22		19.14±0.20					
Synthetic Estimate			(18.96±0.15)	(19.89±0.33)				
Spitzer					16.77±0.03	14.71±0.01		

^a Photometry is on the MKO system except for the TNG Y filter (see text).

^b 95% confidence brightness upper limit.

Table 3. Photometric magnitudes of WISEP J1423+0116.

$Y - J$	$J - H$	$H - K$	$J - K$	$W1 - W2$	$W2 - W3$	$J - W2$	$H - W2$	[3.6] - [4.5]	$H - [4.5]$
0.98±0.07	-0.38±0.23	-0.93±0.36 ^a	-1.27±0.34 ^a	≥2.77 ^b	≤2.55 ^b	3.95±0.10 ^c	4.38±0.22	2.06±0.03	4.43±0.20

^a Synthetic photometry (see text).

^b 95% confidence limit.

^c Using the higher signal-to-noise VISTA J -band magnitude.

Table 4. Photometric colours of WISEP J1423+0116.

7 CONFIRMING BINARITY

To estimate the probability that WISEP J1423+0116 and BD+01 2920 may be a line-of-sight association as opposed to a genuine binary, we have performed a statistical analysis to estimate the expected number of chance alignments in our search. We used the Burningham et al. (2010b) luminosity function constraints to estimate the number of T6-9 dwarfs expected in the WISE first data release. In a sample with $W2 < 15$ (akin to our $W2$ signal-to-noise requirement) we expect to detect T7±1 and T9 dwarfs out to distances (D_{max}) of ~25 and ~15pc respectively, in the 57% sky coverage of the WISE first release. We adjusted the Burningham luminosity function to add back in the correction made for unresolved binarity (3-45%), since this removed T dwarfs from their magnitude limited samples, and estimate an expected 28-251 T7±1 dwarfs and 26-111 T9 dwarfs in the WISE selection using this luminosity function. We then summed the volume in which line-of-sight associated stars may be found using a set of cones (one per T dwarf) each with its apex at the observer and a T dwarf in the centre of its base (using a base radius of 10,000AU to match our search criteria). Since the number of T dwarfs is proportional to D^3 and the volume of a cone is proportional to D (where D is distance), the average cone volume will be $\frac{3}{4}$ of the maximum cone volume $\frac{1}{3}AD_{max}$ (where A is the base area of a cone $\pi \times 10,000AU^2$). The total cone volume for T6-9 dwarfs was thus estimated to be 2.0–14.6pc³.

The luminosity function of Reid et al. (2007) for the 8pc and 20pc samples leads to a stellar density of 0.062–0.076 stars pc⁻³, and we thus expect 0.12–1.11 light-of-sight associations between stars and T dwarfs in our WISE selection. Amongst our five candidates we find that one of them (WISEP J075003.84+272544.8) is in fact a line-of-sight association with a lack of common proper motion. This is consistent with our estimates above. An additional candidate was identified without proper motion, though the above statistic does not provide any further indications on the likelihood that this candidate may be genuine.

We must also assess these common proper motion systems for the chance that common proper motions are aligned by random chance. Using the proper motion and direction of WISEP J1423+0116 we estimated this probability using a Hipparcos sample, downloading the proper motions of Hipparcos stars within 45 degrees of the WISEP J1423+0116/BD+01 2920 pair, and with distances from 10–40pc (the photometric distance range of a T8±1 dwarf with $J \simeq 18.7$ allowing for possible unresolved binarity). We counted the fraction of stars with proper motion within 55mas yr⁻¹ (1σ) of the T dwarf motion, and thus estimate a chance of 1.3% that this high proper motion pair could be common proper motion by random chance. We therefore expect no more than 0.0015–0.014 false positive common proper motion systems in the search that we have made, and conclude that all three of the common proper motion systems that we identified are genuine binaries. This includes the two previously reported systems and the association between WISEP J1423+0116 and BD+01 2920, which becomes the binary system BD+01 2920AB.

8 PROPERTIES OF BD+01 2920A

A search of the literature reveals multiple studies of the primary star BD+01 2920A. It is a nearby high proper motion G1 dwarf (0.9M_⊙) with thin disk kinematics. There is no evidence of any debris disk or low-mass companions (including giant planets), and it has low activity. BD+01 2920A is a mildly metal poor star, with a metallicity in the metal poor tail of the disk distribution rather than in the halo regime. With one exception previous estimates of [Fe/H] are in the range -0.38±0.06 (only Lebreton et al. 1999, gives a slightly higher metallicity of -0.20 dex). The range of age constraints covers 2.3–14.4 Gyr. This differs slightly from the range quoted by Lawler et al. (2009) who give a lower limit of 3.5 Gyr. The difference is due to the estimate of 2.27 Gyr from do Nascimento et al. (2010), and we here adopt

BD+01 2920A (Hip 70319)	
R.A. (J2000)	14 23 15.285
Dec (J2000)	+01 14 29.65
$PM_{\alpha \cos Dec}$	223.8 ± 0.4 mas/yr
PM_{Dec}	-477.4 ± 0.4 mas/yr
Spectral type/class	G1V
π	58.2 ± 0.5 mas ⁽¹⁾
Distance	17.2 ± 0.2 pc
$m - M$	1.18 ± 0.03
V_r	19.6 ± 0.3 km/s ⁽²⁻⁴⁾
Space motion	UVW = 22, 15, 39 ⁽⁵⁻⁸⁾
Population	Thin disk ^(9,10)
T_{eff}	5750 ± 100 K ^(3,7,8,11-21)
$\log g$	4.45 ± 0.05 dex ^(3,7,12,16-18,20-24)
Mass	$0.87 \pm 0.07 M_{\odot}$ ^(3,13,23)
[Fe/H]	-0.38 ± 0.06 dex ^(3,6-8,10,12,14-18,20-29)
Age	2.3 – 14.4 Gyr ^(3,5,8,10,12,13,15,23,26,30-32)
$v \sin i$	1–2 km/s ^(3,12,13)
Activity	Low activity star ⁽³³⁾
Debris disk	None ⁽¹⁵⁾
Close in companions	No $\geq 70\text{-}75 M_{Jup}$ at 20-250AU ⁽³⁴⁾ No giant planets ($>100\text{m/s}$) at $< 5\text{AU}$ ^(24,35-39)

¹ van Leeuwen (2007), ² Gontcharov (2006), ³ Valenti & Fischer (2005)
⁴ Latham et al. (2002), ⁵ Holmberg et al. (2009), ⁶ Ramírez et al. (2007)
⁷ Mishenina et al. (2004), ⁸ Nordström et al. (2004), ⁹ Borkova & Marsakov (2004)
¹⁰ Ibukiyama & Arimoto (2002), ¹¹ Casagrande et al. (2010), ¹² Takeda et al. (2010)
¹³ do Nascimento et al. (2010), ¹⁴ Holmberg et al. (2007), ¹⁵ Lawler et al. (2009)
¹⁶ Luck & Heiter (2006), ¹⁷ Shi et al. (2004), ¹⁸ Mashonkina et al. (2007)
¹⁹ Kovtyukh et al. (2003), ²⁰ Giridhar & Goswami (2002), ²¹ Cayrel de Strobel et al. (2001)
²² Wu et al. (2011), ²³ Takeda et al. (2007b), ²⁴ Heiter & Luck (2003)
²⁵ Mashonkina & Gehren (2001), ²⁶ Rocha-Pinto & Maciel (1998), ²⁷ Karataş et al. (2005)
²⁸ Borkova & Marsakov (2005), ²⁹ Haywood (2001), ³⁰ Wright et al. (2004)
³¹ Barry (1988), ³² Takeda et al. (2007a), ³³ Hall et al. (2007) ³⁴ Carson et al. (2009)
³⁵ Halbwegs et al. (2003), ³⁶ Halbwegs et al. (2000), ³⁷ Cumming et al. (1999)
³⁸ Endl et al. (2002), ³⁹ Nidever et al. (2002)

Table 5. Properties of BD+01 2920A (Hip 70319).

an inclusive age range. The properties of BD+01 2920A are summarised in Table 5 and references therein.

9 PROPERTIES OF BD+01 2920B

9.1 Bolometric flux

We estimate the bolometric flux (F_{bol}) of the new T8p companion BD+01 2920B following a similar method to that outlined in Burningham et al. (2009a), by combining our *YJHK* spectrum (flux calibrated by our follow-up photometry) with model spectra (to allow us to estimate the flux contributions from regions outside our near-infrared spectral coverage). We have scaled the $\lambda < 1.05\mu\text{m}$ region of the models to match the flux level in our *YJHK* spectrum, and we have used the Spitzer 3.6 μm and 4.5 μm photometry to scale the $\lambda = 2.5 - 3.95\mu\text{m}$ and $\lambda > 3.95\mu\text{m}$ regions respectively (the transmission profiles of the Spitzer filters cross at 3.95 μm at a transmission level of $\sim 1\%$). To avoid biasing our derived flux estimate with our choice of model, we have produced estimates using Solar and $[M/H] = -0.3$ metallicity BT Settl models (Allard et al. 2011) that bracket the likely range of gravities and T_{eff} for our target ($\log g =$

4.50 – 5.5; $T_{\text{eff}} = 500 - 900\text{K}$). We take the scatter in the estimates resulting from different model choices as a reflection of the systematic uncertainty introduced by the atmospheric models. We have used a Monte Carlo method to determine the uncertainty in each estimate due to the noise in the photometry used for scaling the models and the noise in our GNIRS spectrum. Our final estimate of F_{bol} is the median of our estimates using different model extensions, whilst the uncertainty is the sum in quadrature of the systematic uncertainty and the mean random uncertainty. This results in a determination of $F_{bol} = 1.61 \pm 0.17 \times 10^{-16} \text{ W m}^{-2}$.

9.2 Luminosity, mass, radius, and effective temperature

The luminosity of BD+01 2920B was derived from the bolometric flux and the distance. The on-sky separation of the BD+01 2920AB components leads to a tangential separation of 0.01 pc. This is negligible compared with the uncertainty in the parallax distance of the primary (± 0.2 pc) and we can therefore assume that the T dwarf is at the same distance as BD+01 2920A (17.2 ± 0.2 pc). Taking the uncertainties associated with the bolometric flux and distance into account

BD+01 2920B (WISEP 1423+0116)	
R.A. (J2000)	14 23 20.86
Dec (J2000)	+01 16 38.1
$PM_{\alpha \cos Dec}$	$261 \pm 56 \text{ mas yr}^{-1}$
PM_{Dec}	$-444 \pm 52 \text{ mas yr}^{-1}$
Spectral type	T8p
Separation	153 arcsecs
	2630 AU ^a
F_{bol}	$(1.61 \pm 0.17) \times 10^{-16} \text{ W m}^{-2}$ ^b
$m - M$	1.18 ± 0.02 ^a
M_Y	18.51 ± 0.04 ^a
M_J	17.53 ± 0.05 ^a
M_H	17.96 ± 0.20 ^a
M_K	18.71 ± 0.33 ^{a,c}
$M_{3.6}$	15.59 ± 0.04 ^a
$M_{4.5}$	13.53 ± 0.02 ^a
$\log L/L_{\odot}$	-5.83 ± 0.05 ^a
$[Fe/H]$	$-0.38 \pm 0.06 \text{ dex}$ ^d
Mass	$0.019 - 0.047 M_{\odot}$ ^e
	$20 - 50 M_{Jup}$ ^e
Radius	$0.080 - 0.099 R_{\odot}$ ^e
	$0.80 - 0.99 R_{Jup}$ ^e
$\log g$	$4.68 - 5.30 \text{ dex}$ ^e
T_{eff}	$680 \pm 55 \text{ K}$ ^f

^a Inferring a distance of $17.2 \pm 0.2 \text{ pc}$ from BD+01 2920A.
^b Integrating measured flux from $1.0 - 2.4 \mu\text{m}$ and adding a theoretical correction at other wavelengths (see text).
^c Synthetic photometry used (see text).
^d Inferred from BD+01 2920A.
^e Constraints derived from structure models as a function of luminosity for ages 210 Gyr.
^f Derived from the luminosity and radius constraints.

Table 6. Properties of BD+01 2920B (WISEP 1423+0116).

leads to the determination of $L_{bol} = 5.69 \pm 0.60 \times 10^{-20} \text{ W}$, or $\log L/L_{\odot} = -5.83 \pm 0.05$. To determine the T_{eff} of BD+01 2920B we estimate its radius using the COND evolutionary models (Baraffe et al. 2003). These models reproduce the main trends of observed methane dwarfs in near-infrared color-magnitude diagrams, though are only available for solar metallicity.

We used linear interpolation between the model isochrones to estimate a range of possible mass, radii and surface gravity for BD+01 2920B consistent with an age range of $\sim 2 - 10$ Gyr. Accounting for the uncertainties in the measured luminosity we obtained a mass range of $0.019 - 0.047 M_{\odot}$ ($20 - 50 M_{Jup}$), a radius range $0.080 - 0.099 R_{\odot}$ ($0.80 - 0.99 R_{Jup}$), and a surface gravity range of $\log g = 4.68 - 5.30$. The corresponding temperature (from luminosity and radius) is $T_{\text{eff}} = 680 \pm 55 \text{ K}$. A summary of the properties of BD+01 2920B is given in Table 6.

Observations of transiting very low-mass stars and brown dwarfs with mass $> 20 M_{Jup}$ (Pont et al. 2005b,a; Deleuil et al. 2008; Bouchy et al. 2011b; Anderson et al. 2011; Johnson et al. 2011) are all consistent with the COND mass-radius model data (see fig 10 of Bouchy et al. 2011a). These systems are solar metallicity to within the uncertainties, though some of these uncertainties are significant. The effects of metallicity on sub-stellar radii are a little unclear. Burrows et al. (2011) present evolutionary models with a spread in radius (at a given mass and age) of $\sim 10 - 25\%$, with

higher-metallicity (higher-cloud-thickness) atmospheres giving larger radii. However, a comparison between KOI-423b and CoRoT-3b suggests the converse trend. KOI-423b orbits a metal poor star ($[Fe/H] = -0.29 \pm 0.10$) and is a relatively large ($1.22^{+0.12}_{-0.10} R_{Jup}$) brown dwarf ($18 M_{Jup}$), whereas CoRoT-3 is a solar metallicity star ($[Fe/H] = -0.02 \pm 0.06$) hosting a smaller ($1.01 \pm 0.07 R_{Jup}$) brown dwarf ($22 M_{Jup}$). Given this uncertainty in the radius-metallicity trend, we do not attempt to make a metallicity correction to our radius estimate. We note however that our COND radius constraint already includes an uncertainty at the level of 25%, comparable with the size of the theoretical trends suggested by the Burrows et al. (2011) models for a metallicity difference of 1.0 dex.

As an additional caveat we note that our T_{eff} determination relies on an assumption that the object is single, and not an unresolved binary. Unresolved binarity would lead to lower T_{eff} for each unresolved component. If BD+01 2920B is an equal luminosity unresolved binary the T_{eff} of each component would be a factor ~ 0.8 less ($\frac{1}{2}^{\frac{1}{4}}$ with similar radii for the components). For unequal luminosity components the brighter component T_{eff} would be closer to 680K with the fainter one $< 540 \text{ K}$. Observations suggest (e.g. Burgasser et al. 2005) that the binary fraction of brown dwarfs (resolved at ~ 0.1 arcsec resolution) in widely separated stellar – brown dwarf multiples is notably higher (45 ± 15 per cent) than that of field brown dwarfs (18 ± 7 per cent), and unresolved binaries can also have separation closer than 0.1 arcseconds (see Burningham et al. 2009a, and references therein). In Figure 3 we show BD+01 2920B in absolute magnitude ($M_{J,H,K}$) spectral type diagrams, along with the known population of late T and Y dwarfs (see caption). The K-band suppression is evident in the M_K plot, though we also note that there is no clear indication that the object is an unresolved binary (e.g. with components of near equal brightness) in the M_J and M_H plots. We cannot with high confidence however, rule out the possibility that BD+01 2920B is an unresolved binary.

10 A METAL POOR BENCHMARK T8 DWARF

We now assess some implications of this benchmark system under the assumption that it is a single object, and through comparison of its spectrum and colours to theoretical predictions and other ultra-cool objects. In Figure 4 we compare our flux calibrated GNIRS spectrum of BD+01 2920B and warm-*Spitzer* photometry to mildly metal poor BT Settl models (Allard et al. 2010) for our derived properties, each scaled to their corresponding radii and the known distance to the primary star. The BT Settl atmospheric model grid spans the cool stellar to substellar temperature regime using the BT2 water line-list (Barber et al. 2006) and the reference Solar abundances of Asplund et al. (2009). In these models dust formation, cloud behaviour and vertical mixing are parameterised with reference to the 2D radiation hydrodynamic simulations of Freytag et al. (2010). The K-band suppression that is predicted by the models for high-gravity and metal poorer brown dwarfs is seen in our GNIRS spectrum of this benchmark T dwarf, although the models predict this effect to be stronger than is seen in

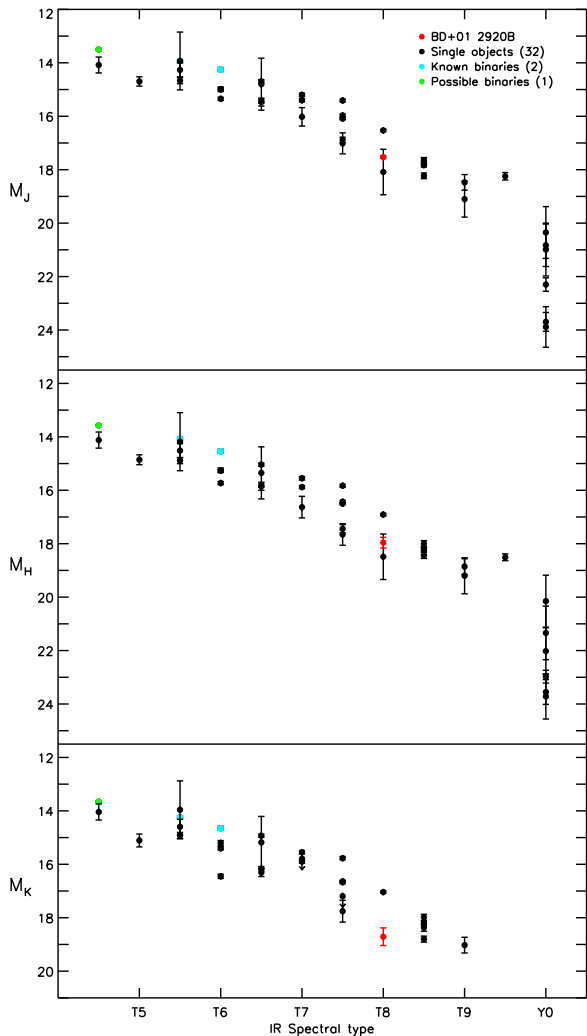


Figure 3. Absolute magnitude ($M_{J,H,K}$) spectral type plots showing BD+01 2920B (red symbol) amongst the existing population of mid-late T dwarfs and Y dwarfs. All the T dwarfs with spectral types $\leq T8.5$ (Burningham et al. 2008) have distances from parallax. The T9.5 and Y dwarfs all have spectroscopic distances (except for WISEP J1541-2250 which has a parallax in Kirkpatrick et al. 2011), estimated via T_{eff} and $\log g$ constraints from model fits to near-infrared spectroscopy.

this case. Similarly poor matches to the observed K -band spectroscopy have been seen in other benchmark systems (e.g. Burningham et al. 2009b, 2011b), so it is reasonable to interpret this as a deficiency in the model atmospheres, although its origin is not yet understood. It is noteworthy that the Y -band spectrum which has also been proposed as diagnostic of metallicity variations (Burgasser et al. 2006a) is also poorly matched by the models. The model atmospheres provide good matches to the flux in the J - and H -bands, despite known deficiencies in the methane line lists in these regions. The model predictions for the [3.6] and [4.5] fluxes are consistent with those that we have observed, and it interesting to note that in the [3.6] band, the 620K, $\log g = 4.7$, model fits the data best, whilst in the [4.5] band the two warmer models provide the best match.

In Figure 5 we have plotted synthetic colours in

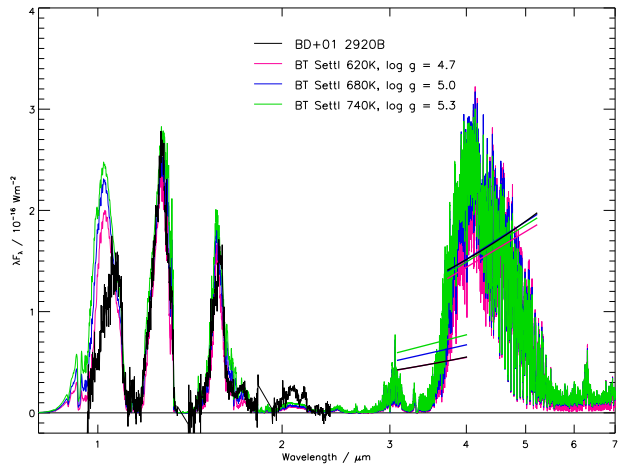


Figure 4. The $YJHK$ spectrum of BD+01 2920B and mean fluxes inferred from the Spitzer photometry compared to model spectra that straddle the properties estimated in Section 9.2. The straight coloured lines indicate the mean fluxes of model spectra in the IRAC channel 1 and 2 photometric bands and are plotted to allow comparison with the mean flux from the target (straight black lines) through the same filters.

$H - K$ and $H - [4.5]$ for the BT Settl models along with colours of late T dwarfs from Leggett et al. (2010b) with MKO and IRAC photometry, and BD+01 2920B. It can be seen that BD+01 2920B lies in a similar region as other suspected mildly metal-poor T7.5/8 dwarfs 2MASS0939 and SDSS1416B, which have $T_{\text{eff}} 500\text{--}700\text{K}$ (e.g. Burningham et al. 2010a; Leggett et al. 2010a). The effect of the poor match between the models and the data in the K -band is highlighted by the non-coincidence of the models and the observations in this colour space for the T dwarfs with the reddest $H - [4.5]$ colours. However, the models correctly predict the colours for the young benchmark Ross 458C. To provide an alternative comparison between the models and the data we have shifted the model colours such that they match the observed colours for BD+01 2920B for the parameters derived in Section 9. Figure 6 compares these adjusted model colours to the same T dwarfs shown in Figure 5. This plot broadly reproduces the result of Leggett et al. (2010b), where it was noted that the majority of the coolest T dwarfs appear to have low-gravity and/or high-metallicity, suggesting that the sample is dominated by young low-mass brown dwarfs (ages $\sim 1\text{Gyr}$). However, we note that the sources with bluer $H - [4.5]$ lie well below the adjusted model tracks in Figure 6, including the young benchmark Ross 458C (for which $\log g = 4.0 - 4.7$; Burningham et al. 2011a), which highlights that a simple offset correction to the models is not sufficient to allow the properties of the T dwarf population to be reliably assessed through reference to these model colours. The similar temperature of these two benchmarks ($T_{\text{eff}} \sim 700\text{K}$), but wide separation in Figures 5 and 6 highlights the important roles that gravity and metallicity play in determining the $H - K/H - [4.5]$ colours for cool T dwarfs.

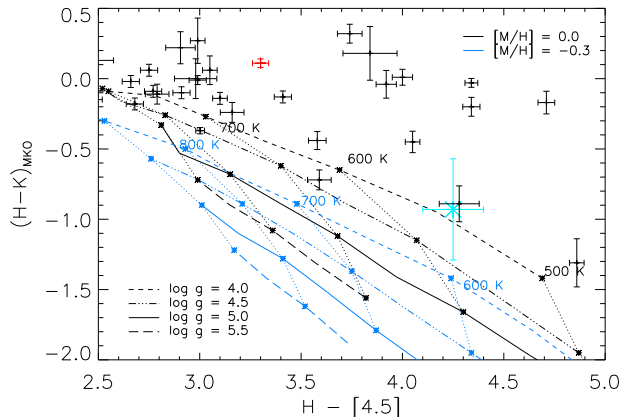


Figure 5. Near- to mid-infrared colours of cool T dwarfs compared to those of the BT Settl model colours. BD+01 2920B is indicated with a cyan star symbol, whilst the young benchmark Ross 458C is indicated in red.

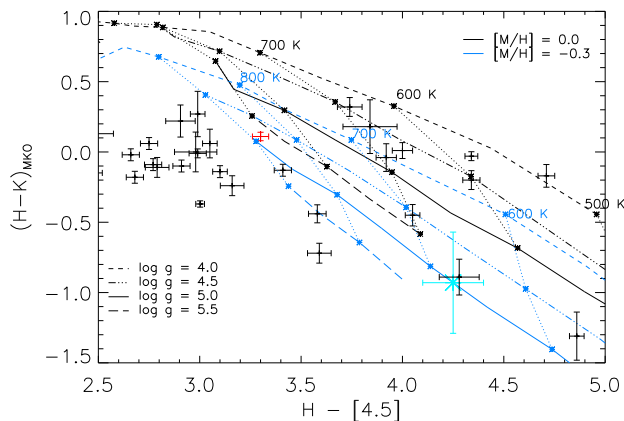


Figure 6. Near- to mid-infrared colours of cool T dwarfs compared to those of the BT Settl model colours anchored to our estimated properties for BD+01 2920B. BD+01 2920B is indicated with a cyan star symbol, whilst the young benchmark Ross 458C is indicated in red.

11 CONCLUSIONS AND FUTURE WORK

Our cross-match between the WISE first data release and the Hipparcos and Gliese catalogues has resulted in the discovery of a new late T binary companion (BD+012920B) and the re-discovery of two previously known systems. WISE (in combination with UKIDSS and VISTA) is thus effectively probing an increased volume of very low temperature parameter-space for benchmark companions. There are also significant advantages that the primary star BD+012920A is a nearby G dwarf rather than one of the more numerous M dwarfs in the solar neighbourhood, and its lower metallicity provides a crucial test for the effects of reduced metal content on models atmospheres. The metallicities and abundances of bright Sun-like stars can be studied with much more confidence and in much greater detail than those of M dwarfs, and late T dwarfs in such systems offer the opportunity not only to test cool brown dwarf atmosphere physics, but also to potentially study brown dwarf abundances.

In the near future, high resolution imaging (e.g. adap-

tive optics) observations of BD+012920B will be important to constrain multiplicity on a ~ 0.1 arcsec (~ 1.7 AU) separation scale. A close binary would be able to provide future dynamical masses (since the orbital period would be just a few years). Higher resolution spectroscopy would also be able to assess multiplicity at closer separation, and confirmation of a single object nature would validate the approach taken here to determination the physical properties of this benchmark object. The existing constraints on the physical properties of BD+012920B will be improved as we develop a better understanding of how brown dwarf radii depend on composition. This will be aided by an increasing number of transiting brown dwarfs from Kepler and other transit surveys (e.g. Borucki et al. 2011; Pinfield et al. 2005), and improved metallicity measurements for this sample.

We can expect additional late T benchmarks in the future all-sky WISE data release, and a more encompassing search of WISE, UKIDSS and VISTA (including at wider angular separations) should yield an expanded population of benchmarks across the full T dwarf T_{eff} range. As greater survey volumes are searched for benchmark brown dwarfs we can also expect to identify systems with more accurately known ages. Evolved subgiants for example are less numerous than their main sequence counterparts, but evolutionary model comparisons can provide more accurate age constraints (e.g. $\pm 10\%$; Pinfield et al. 2006). And as the range of well measured benchmarks expands into greater parameter-space we will have the opportunity to comprehensively test the atmosphere models by directly mapping the benchmark population’s spectral variations/trends onto a grid of tightly constrained physical properties.

ACKNOWLEDGMENTS

This publication makes use of data products from the Wide-field Infrared Survey Explorer, which is a joint project of the University of California, Los Angeles, and the Jet Propulsion Laboratory/California Institute of Technology, funded by the National Aeronautics and Space Administration. The UKIDSS project is defined in Lawrence et al. (2007). UKIDSS uses the UKIRT WFCAM (Casali et al. 2007) and a photometric system described in Hewett et al. (2006). The pipeline processing and science archive are described in Irwin et al. (2004) and Hambly et al. (2008). Based on observations obtained at the Gemini Observatory, which is operated by the Association of Universities for Research in Astronomy, Inc., under a cooperative agreement with the NSF on behalf of the Gemini partnership: the National Science Foundation (United States), the Science and Technology Facilities Council (United Kingdom), the National Research Council (Canada), CONICYT (Chile), the Australian Research Council (Australia), Ministério da Ciência, Tecnologia e Inovação (Brazil) and Ministerio de Ciencia, Tecnología e Innovación Productiva (Argentina). This work made use of data obtained on Gemini projects GN-2011A-Q-73. Based in part on observations made for the VIKING survey, using VISTA at the ESO Paranal Observatory under programme ID 179.A-2004. The VISTA Data Flow System pipeline processing and science archive are described in Irwin et al (2004) and Hambly et al (2008). Based on observations made with the Italian Telescopio Nazionale Galileo (A22TAC96) oper-

ated on the island of La Palma by the Fundación Galileo Galilei of the INAF (Istituto Nazionale di Astrofisica) at the Spanish Observatorio del Roque de los Muchachos of the Instituto de Astrofisica de Canarias. DP, NL, PL, MCG and ZZ have received support from RoPACS during this research and JG is supported by RoPACS, a Marie Curie Initial Training Network funded by the European Commissions Seventh Framework Programme. NL is funded by the national program AYA2010-19136 funded by the Spanish ministry of science and innovation. SKL is supported by the Gemini Observatory, which is operated by AURA, on behalf of the international Gemini partnership of Argentina, Australia, Brazil, Canada, Chile, the United Kingdom, and the United States of America. ADJ is supported by a Fondecyt Postdoctorado under project number 3100098. JSJ is supported by a Fondecyt Postdoctorado under project number 3110004 and partial support from Centro de Astrofísica FONDAP 15010003, the GEMINI-CONICYT FUND and from the Comité Mixto ESO-GOBIERNO DE CHILE. This research has made use of the SIMBAD database, operated at CDS, Strasbourg, France.

REFERENCES

- Allard F., Hauschildt P. H., Alexander D. R., Starrfield S., 1997, *ARA&A*, 35, 137
- Allard F., Hauschildt P. H., Alexander D. R., Tamanai A., Schweitzer A., 2001, *ApJ*, 556, 357
- Allard F., Homeier D., Freytag B., 2010, *ArXiv e-prints*
- Allard F., Homeier D., Freytag B., 2011, *PTRSA*, accepted
- Anderson D. R. et al., 2011, *ApJ*, 726, L19
- Asplund M., Grevesse N., Sauval A. J., Scott P., 2009, *ARA&A*, 47, 481
- Baffa C. et al., 2001, *A&A*, 378, 722
- Baraffe I., Chabrier G., Barman T. S., Allard F., Hauschildt P. H., 2003, *A&A*, 402, 701
- Barber R. J., Tennyson J., Harris G. J., Tolchenov R. N., 2006, *MNRAS*, 368, 1087
- Barry D. C., 1988, *ApJ*, 334, 436
- Bate M. R., Bonnell I. A., Bromm V., 2002, *MNRAS*, 332, L65
- Bohlin R. C., Gilliland R. L., 2004, *AJ*, 127, 3508
- Borkova T. V., Marsakov V. A., 2004, *Astronomy Letters*, 30, 148
- Borkova T. V., Marsakov V. A., 2005, *Astronomy Reports*, 49, 405
- Borucki W. J. et al., 2011, *ApJ*, 736, 19
- Bouchy F. et al., 2011a, *A&A*, 533, A83
- Bouchy F. et al., 2011b, *A&A*, 525, A68
- Burgasser A. J., Burrows A., Kirkpatrick J. D., 2006a, *ApJ*, 639, 1095
- Burgasser A. J., Geballe T. R., Leggett S. K., Kirkpatrick J. D., Golimowski D. A., 2006b, *ApJ*, 637, 1067
- Burgasser A. J. et al., 2002, *ApJ*, 564, 421
- Burgasser A. J. et al., 2000, *ApJ*, 531, L57
- Burgasser A. J., Kirkpatrick J. D., Lowrance P. J., 2005, *AJ*, 129, 2849
- Burningham B. et al., 2011a, *MNRAS*, 414, 3590
- Burningham B. et al., 2011b, *MNRAS*, 414, 3590
- Burningham B. et al., 2010a, *MNRAS*, 404, 1952
- Burningham B. et al., 2011c, *MNRAS*, 414, L90
- Burningham B. et al., 2008, *MNRAS*, 391, 320
- Burningham B. et al., 2009a, *MNRAS*, 395, 1237
- Burningham B. et al., 2009b, *MNRAS*, 395, 1237
- Burningham B. et al., 2010b, *MNRAS*, 406, 1885
- Burrows A., Heng K., Nampaisarn T., 2011, *ApJ*, 736, 47
- Carson J. C., Hiner K. D., Villar, III G. G., Blaschak M. G., Rudolph A. L., Stapelfeldt K. R., 2009, *AJ*, 137, 218
- Casagrande L., Ramírez I., Meléndez J., Bessell M., Asplund M., 2010, *A&A*, 512, A54
- Cayrel de Strobel G., Soubiran C., Ralite N., 2001, *A&A*, 373, 159
- Clarke J. R. A. et al., 2010, *MNRAS*, 402, 575
- Cooke A., Rodgers B., 2005, in *Astronomical Society of the Pacific Conference Series*, Vol. 347, *Astronomical Data Analysis Software and Systems XIV*, P. Shopbell, M. Britton, & R. Ebert, ed., pp. 514+–
- Cumming A., Marcy G. W., Butler R. P., 1999, *ApJ*, 526, 890
- Cushing M. C. et al., 2011, *ArXiv e-prints*
- Day-Jones A. C. et al., 2011, *MNRAS*, 410, 705
- Deleuil M. et al., 2008, *A&A*, 491, 889
- Delorme P. et al., 2008, *A&A*, 482, 961
- do Nascimento J. D., da Costa J. S., de Medeiros J. R., 2010, *A&A*, 519, A101
- Elias J. H., Joyce R. R., Liang M., Muller G. P., Hileman E. A., George J. R., 2006, in *Presented at the Society of Photo-Optical Instrumentation Engineers (SPIE) Conference*, Vol. 6269, *Society of Photo-Optical Instrumentation Engineers (SPIE) Conference Series*
- Endl M., Kürster M., Els S., Hatzes A. P., Cochran W. D., Dennerl K., Döbereiner S., 2002, *A&A*, 392, 671
- Epchtein N. et al., 1997, *The Messenger*, 87, 27
- Faherty J. K., Burgasser A. J., West A. A., Bochanski J. J., Cruz K. L., Shara M. M., Walter F. M., 2010, *AJ*, 139, 176
- Freytag B., Allard F., Ludwig H., Homeier D., Steffen M., 2010, *A&A*, 513, A19+
- Gálvez-Ortiz M. C. et al., 2010, *MNRAS*, 409, 552
- Giridhar S., Goswami A., 2002, *Bulletin of the Astronomical Society of India*, 30, 501
- Gliese W., Jahreiss H., 1991, *NASA STI/Recon Technical Report A*, 923, 33932
- Gontcharov G. A., 2006, *Astronomy Letters*, 32, 759
- Goodwin S. P., Whitworth A., 2007, *A&A*, 466, 943
- Halbwachs J. L., Arenou F., Mayor M., Udry S., Queloz D., 2000, *A&A*, 355, 581
- Halbwachs J. L., Mayor M., Udry S., Arenou F., 2003, *A&A*, 397, 159
- Hall J. C., Lockwood G. W., Skiff B. A., 2007, *AJ*, 133, 862
- Haywood M., 2001, *MNRAS*, 325, 1365
- Heiter U., Luck R. E., 2003, *AJ*, 126, 2015
- Hewett P. C., Warren S. J., Leggett S. K., Hodgkin S. T., 2006, *MNRAS*, 367, 454
- Holmberg J., Nordström B., Andersen J., 2007, *A&A*, 475, 519
- Holmberg J., Nordström B., Andersen J., 2009, *A&A*, 501, 941
- Ibukiyama A., Arimoto N., 2002, *A&A*, 394, 927
- Johnson J. A. et al., 2011, *ApJ*, 730, 79
- Karataş Y., Bilir S., Schuster W. J., 2005, *MNRAS*, 360, 1345

- Kirkpatrick J. D., 2005, *ARA&A*, 43, 195
- Kirkpatrick J. D. et al., 2011, ArXiv e-prints
- Knapp G. R. et al., 2004, *AJ*, 127, 3553
- Kovtyukh V. V., Soubiran C., Belik S. I., Gorlova N. I., 2003, *A&A*, 411, 559
- Latham D. W., Stefanik R. P., Torres G., Davis R. J., Mazeh T., Carney B. W., Laird J. B., Morse J. A., 2002, *AJ*, 124, 1144
- Lawler S. M. et al., 2009, *ApJ*, 705, 89
- Lawrence A. et al., 2007, *MNRAS*, 379, 1599
- Lebreton Y., Perrin M.-N., Cayrel R., Baglin A., Fernandes J., 1999, *A&A*, 350, 587
- Leggett S. K. et al., 2010a, *ApJ*, 710, 1627
- Leggett S. K. et al., 2010b, *ApJ*, 710, 1627
- Leggett S. K. et al., 2006, *MNRAS*, 373, 781
- Leggett S. K., Saumon D., Burningham B., Cushing M. C., Marley M. S., Pinfield D. J., 2010c, *ApJ*, 720, 252
- Liu M. C., Leggett S. K., Chiu K., 2007, *ApJ*, 660, 1507
- Lodieu N. et al., 2007, *MNRAS*, 379, 1423
- Lucas P. W. et al., 2010, *MNRAS*, 408, L56
- Luck R. E., Heiter U., 2006, *AJ*, 131, 3069
- Mainzer A. et al., 2011, *ApJ*, 726, 30
- Mashonkina L., Gehren T., 2001, *A&A*, 376, 232
- Mashonkina L., Korn A. J., Przybilla N., 2007, *A&A*, 461, 261
- Mishenina T. V., Soubiran C., Kovtyukh V. V., Korotin S. A., 2004, *A&A*, 418, 551
- Munn J. A. et al., 2004, *AJ*, 127, 3034
- Murray D. N. et al., 2011, *MNRAS*, 414, 575
- Nidever D. L., Marcy G. W., Butler R. P., Fischer D. A., Vogt S. S., 2002, *ApJS*, 141, 503
- Nordström B. et al., 2004, *A&A*, 418, 989
- Pinfield D. J. et al., 2008, *MNRAS*, 390, 304
- Pinfield D. J., Jones H. R. A., Lucas P. W., Kendall T. R., Folkes S. L., Day-Jones A. C., Chappelle R. J., Steele I. A., 2006, *MNRAS*, 368, 1281
- Pinfield D. J., Jones H. R. A., Steele I. A., 2005, *PASP*, 117, 173
- Pont F., Bouchy F., Melo C., Santos N. C., Mayor M., Queloz D., Udry S., 2005a, *A&A*, 438, 1123
- Pont F., Melo C. H. F., Bouchy F., Udry S., Queloz D., Mayor M., Santos N. C., 2005b, *A&A*, 433, L21
- Ramírez I., Allende Prieto C., Lambert D. L., 2007, *A&A*, 465, 271
- Reid I. N., Cruz K. L., Allen P. R., 2007, *AJ*, 133, 2825
- Reylé C. et al., 2010, *A&A*, 522, A112
- Rocha-Pinto H. J., Maciel W. J., 1998, *MNRAS*, 298, 332
- Saumon D., Bergeron P., Lunine J. I., Hubbard W. B., Burrows A., 1994, *ApJ*, 424, 333
- Saumon D. et al., 2007, *ApJ*, 656, 1136
- Scholz R.-D., 2010, *A&A*, 515, A92
- Shi J. R., Gehren T., Zhao G., 2004, *A&A*, 423, 683
- Skrutskie M. F. et al., 2006, *AJ*, 131, 1163
- Stamatellos D., Hubber D. A., Whitworth A. P., 2007, *MNRAS*, 382, L30
- Sumi T. et al., 2011, *Nature*, 473, 349
- Takeda G., Ford E. B., Sills A., Rasio F. A., Fischer D. A., Valenti J. A., 2007a, *ApJS*, 168, 297
- Takeda Y., Honda S., Kawanomoto S., Ando H., Sakurai T., 2010, *A&A*, 515, A93
- Takeda Y., Kawanomoto S., Honda S., Ando H., Sakurai T., 2007b, *A&A*, 468, 663
- Valenti J. A., Fischer D. A., 2005, *ApJS*, 159, 141
- van Leeuwen F., 2007, *A&A*, 474, 653
- Warren S. J. et al., 2007, *MNRAS*, 381, 1400
- Wright E. L. et al., 2010, *AJ*, 140, 1868
- Wright J. T., Marcy G. W., Butler R. P., Vogt S. S., 2004, *ApJS*, 152, 261
- Wu Y., Singh H. P., Prugniel P., Gupta R., Koleva M., 2011, *A&A*, 525, A71
- York D. G. et al., 2000, *AJ*, 120, 1579
- Zhang Z. H. et al., 2010, *MNRAS*, 404, 1817